

ORIGINAL RESEARCH

Pharmacologic TWIK-Related Acid-Sensitive K⁺ Channel (TASK-1) Potassium Channel Inhibitor A293 Facilitates Acute Cardioversion of Paroxysmal Atrial Fibrillation in a Porcine Large Animal Model

Felix Wiedmann, MD; Christoph Beyersdorf, BSc; Xiaobo Zhou, MD; Antonius Büscher, MD; Manuel Kraft, MSc; Jendrik Nietfeld, BSc; Teo Puig Walz, MSc; Laura A. Unger, MSc; Axel Loewe, PhD; Bastian Schmack, MD; Arjang Ruhparwar, MD; Matthias Karck, MD; Dierk Thomas, MD; Martin Borggreffe, MD; Gunnar Seemann, PhD; Hugo A. Katus, MD; Constanze Schmidt, MD

BACKGROUND: The tandem of P domains in a weak inward rectifying K⁺ channel (TWIK)-related acid-sensitive K⁺ channel (TASK-1; hK_{2p}3.1) two-pore-domain potassium channel was recently shown to regulate the atrial action potential duration. In the human heart, TASK-1 channels are specifically expressed in the atria. Furthermore, upregulation of atrial TASK-1 currents was described in patients suffering from atrial fibrillation (AF). We therefore hypothesized that TASK-1 channels represent an ideal target for antiarrhythmic therapy of AF. In the present study, we tested the antiarrhythmic effects of the high-affinity TASK-1 inhibitor A293 on cardioversion in a porcine model of paroxysmal AF.

METHODS AND RESULTS: Heterologously expressed human and porcine TASK-1 channels are blocked by A293 to a similar extent. Patch clamp measurements from isolated human and porcine atrial cardiomyocytes showed comparable TASK-1 currents. Computational modeling was used to investigate the conditions under which A293 would be antiarrhythmic. German landrace pigs underwent electrophysiological studies under general anesthesia. Paroxysmal AF was induced by right atrial burst stimulation. After induction of AF episodes, intravenous administration of A293 restored sinus rhythm within cardioversion times of 177±63 seconds. Intravenous administration of A293 resulted in significant prolongation of the atrial effective refractory period, measured at cycle lengths of 300, 400 and 500 ms, whereas the surface ECG parameters and the ventricular effective refractory period lengths remained unchanged.

CONCLUSIONS: Pharmacological inhibition of atrial TASK-1 currents exerts antiarrhythmic effects in vivo as well as in silico, resulting in acute cardioversion of paroxysmal AF. Taken together, these experiments indicate the therapeutic potential of A293 for AF treatment.

Key Words: A293 ■ antiarrhythmic pharmacotherapy ■ atrial fibrillation ■ cardioversion ■ K_{2p}3.1 ■ TASK-1

Atrial fibrillation (AF) is the most common sustained arrhythmia and represents a major risk factor for stroke, acute heart failure and cardiovascular morbidity.¹ In the Western world, ≈2% of the population

suffers from paroxysmal, persistent, or permanent AF. The prevalence and incidence of AF increase with age. It was predicted that the number of patients with AF will significantly rise in our aging population.² Despite

Correspondence to: Constanze Schmidt, MD, FESC, SOT, Department of Cardiology, Medical University Hospital Heidelberg, Im Neuenheimer Feld 410, D-69120 Heidelberg, Germany. E-mail: constanze.schmidt@med.uni-heidelberg.de

Supplementary Materials for this article are available at <https://www.ahajournals.org/doi/suppl/10.1161/JAHA.119.015751>

For Sources of Funding and Disclosures, see page 15.

© 2020 The Authors. Published on behalf of the American Heart Association, Inc., by Wiley. This is an open access article under the terms of the Creative Commons Attribution-NonCommercial-NoDerivs License, which permits use and distribution in any medium, provided the original work is properly cited, the use is non-commercial and no modifications or adaptations are made.

JAHA is available at: www.ahajournals.org/journal/jaha

CLINICAL PERSPECTIVE

What Is New?

- Tandem of P domains in a weak inward rectifying K⁺ channel (TWIK)-related acid-sensitive K⁺ channel (TASK-1) background potassium channels, which were recently described to be up-regulated in patients with atrial fibrillation display comparable atrial-specific expression patterns in the human and the porcine heart.
- Our preclinical in vivo study shows that pharmacological inhibition of TASK-1 can be employed for fast and safe cardioversion of new-onset atrial fibrillation episodes.

What Are the Clinical Implications?

- TASK-1 inhibition might extend our options for pharmacological atrial fibrillation therapy.
- Atrial-specific antiarrhythmic effects of TASK-1 inhibition lack proarrhythmogenic ventricular side effects.

Nonstandard Abbreviations and Acronyms

A293	2-(butylsulfonylamino)-N-[(1R)-1-(6-methoxy-3-pyridyl)propyl]-benzamide
ACTB	β-actin
AERP	atrial effective refractory period
AF	atrial fibrillation
APD	action potential duration
BCL	basic cycle length
K_{2P}	two-pore-domain potassium channel
TASK	TWIK-related acid-sensitive K ⁺ channel
TWIK	tandem of P domains in a weak inward rectifying K ⁺ channel

the epidemiologic and individual relevance of AF, current pharmacologic, interventional, or surgical therapeutic strategies show suboptimal effectiveness and frequently cause severe adverse events.³ Currently, safe and effective management of AF remains an unmet medical need.

Tandem of P domains in a weak inward rectifying K⁺ channel (TWIK)-related acid-sensitive K⁺ channel (TASK-1; K_{2P}3.1) is a member of the two-pore-domain potassium (K_{2P}-) channel family. K_{2P} channels are the most recently discovered family of K⁺ channels.⁴ The 15 members of the K_{2P} family are abundantly expressed throughout the body and are implicated in several physiological processes, including the regulation of cardiac rhythm, blood pressure, neuroprotection, anesthesia, and

apoptosis, as well as the sensation of oxygen tension, mechanical stress, taste, and temperature.^{5–9} In cardiomyocytes, K_{2P} channels mediate action potential repolarization. In particular, TASK-1 currents were recently shown to modulate atrial action potential duration (APD) in AF and heart failure.^{10,11} In the human heart, the expression of TASK-1 subunits is restricted to the atria.^{10,12,13} Strikingly, the atrial TASK-1 levels were upregulated in paroxysmal and chronic AF, which contributes to pathological shortening of the atrial APD.¹⁰ In vitro experiments demonstrated that pharmacologic blockade of TASK-1 currents could revert the APD shortening observed in atrial cardiomyocytes isolated from patients with AF to levels observed among controls with sinus rhythm.¹⁰ Therefore, TASK-1 inhibition may represent an atrial-specific, mechanism-based approach for AF therapy.^{14,15}

The aromatic carbonamide A293 was initially developed as an inhibitor of the K_v1.5 channel by Sanofi-Aventis (Frankfurt, Germany). This experimental compound was later found to be a much more potent TASK-1 inhibitor that is active in the 3-digit nanomolar range.^{16–18}

This preclinical study was designed as a proof-of-concept trial to assess the antiarrhythmic potential of the pharmacologic TASK-1 K⁺ channel inhibitor A293 for acute cardioversion in a porcine model of AF as well as in a translational in silico model of human atrial electrophysiology.

METHODS

Data, Materials, and Code Disclosure Statement

The data that support the findings of this study are available from the corresponding author upon request.

Ethics Statement

The study protocol involving human tissue samples was approved by the ethics committees of the University of Heidelberg (Germany; Medical Faculty Heidelberg, S-017/2013; Medical Faculty Mannheim, 2011-216 N-MA). Written informed consent was obtained from all patients, and the study was conducted in accordance with the Declaration of Helsinki. Animal experiments were carried out in accordance with the *Guide for the Care and Use of Laboratory Animals* as adopted and promulgated by the US National Institutes of Health (NIH publication no. 86-23, revised 1985), with European Union Directive 2010/63/EU, and with the current version of the German Law on the Protection of Animals. Approval for experiments involving animals was granted by the local Animal Welfare Committee (Regierungspraesidium

Karlsruhe, Germany, reference numbers A-38/11, G-221/12, G-296/14, and G-217/18).

Animal Handling

Electrophysiological studies were performed in 17 anesthetized pigs of both sexes (<6 months of age; body weight 30–45 kg). After sedation with azaperon (5 mg/kg IM; Elanco, Bad Homburg, Germany), midazolam (1 mg/kg IM; Hameln Pharma Plus GmbH, Hameln, Germany), and ketamine (10 mg/kg IM; Zoetis Deutschland GmbH, Berlin, Germany), animals were anesthetized with propofol (1.5 mg/kg IV bolus followed by 4–8 mg/kg/h IV; Fresenius Kabi, Bad Homburg, Germany). For analgesia, buprenorphine (0.02 mg/kg IV; Bayer Vital GmbH Tiergesundheit, Leverkusen, Germany) was administered. Mechanical ventilation was performed using the Draeger Primus system (Draeger, Luebeck, Germany). Before surgical jugular vein preparation, a single dose of cefuroxime was administered (750 mg IV; Ratiopharm GmbH, Ulm, Germany). No volatile anesthetics were used to avoid pharmacologic interaction with cardiac K_{2P} channels. Pigs were kept under specific pathogen-free conditions at a room temperature of $20^{\circ}\text{C}\pm 2^{\circ}\text{C}$ with a maximum housing density according to directive 2010/63/EU. Room lighting had a light/dark cycle of 12/12 h. Water was offered ad libitum and pigs were fed twice a day with balanced complete feed (SAF 130M, ZG Raiffeissen, Karlsruhe, Germany). Environmental enrichment was provided with biting woods, chains, and feeding balls.

Electrophysiological Examination

After cannulation of the right jugular vein, quadripolar catheters were placed under fluoroscopic guidance at the junction of the superior vena cava to the right atrium and in the right ventricular apex. A UHS 20 stimulus generator (Biotronik, Berlin, Germany) was used for intracardiac stimulation and the EP Lab duo system (Bard Electrophysiology Division, Lowell, MA) was used for recording, analyzing, and storing ECGs. If induction of AF episodes required electrical cardioversion, electrophysiological studies were paused for at least 30 minutes afterwards.

Pacing thresholds ranged from 0.5 to 2 V at 2.9 ms, and stimulation was performed at twice the diastolic pacing threshold. For measurements of effective refractory periods, a conditioning train of 9 basic stimuli (S1) was followed by a diastolic extrastimulus (S2) starting 150 ms longer than the expected effective refractory period. Coupling intervals of extrastimuli were decreased in 10-ms decrements until refractoriness of the S2 stimulus was achieved. The shortest coupling interval eliciting a propagated atrial response was taken as the effective refractory period.

Surface ECGs were recorded using conventional adhesive electrodes (3M red dot, 3M, Maplewood, MN) in the classical Einthoven /Goldberger /chest-lead configurations, and QT intervals were corrected using Bazett's formula.¹⁹

Porcine Model of Acute Paroxysmal AF

AF was induced via right atrial burst stimulation (2- to 8-second bursts, at 400/min to 1200/min, 10 V, 2.9 ms duration). Upon induction of AF episodes, atrial rhythm was monitored for 5 minutes to probe stability of the AF episode. Pigs that still remained in AF after this 5-minute period were subjected to treatment with A293 or respective vehicle controls. Time to conversion was monitored. When a pig remained in AF >10 minutes, an electrical cardioversion was performed. No further pharmacologic experiments were performed on individual animals for at least 8 plasma half-life times of A293.

Drug Administration

The aromatic carbonamide A293 2-(butylsulfonfylamino)-N-[(1R)-1-(6-methoxy-3-pyridyl)propyl]-benzamide synthesized by ChiroBlock (ChiroBlock, Wolfen, Germany) with a purity of 98%, was dissolved in dimethyl sulfoxide to a concentration of 10 mmol/L and stock solutions were stored at -20°C . During experiments, 1 mg/kg body weight of A293 was administered as short infusion (100 mL 0.9% NaCl) over 5 minutes.

Cardiomyocyte Isolation and Patch Clamp Measurements

After transport in chilled Ca^{2+} -free solution (100 mmol/L NaCl, 10 mmol/L KCl, 1.2 mmol/L KH_2PO_4 , 5 mmol/L MgSO_4 , 50 mmol/L taurine, 5 mmol/L 3-(N-morpholino)propanesulfonic acid, 30 mmol/L 2,3-butanedione monoxime and 20 mmol/L glucose, pH 7.0 with NaOH), right atrial human or porcine tissue samples were dissected into small chunks and rinsed 3 times for 3 minutes with Ca^{2+} -free Tyrode's solution. All solutions were oxygenated with 100% O_2 at 37°C . Subsequently, tissue pieces were subjected to digestion with collagenase type I, 288 U/mL (Worthington Biochemical Corporation, Lakewood, NJ) and protease type XXIV, 5 mg/mL (Sigma-Aldrich) in Ca^{2+} -free Tyrode's solution for 15 minutes. The Ca^{2+} concentration was then increased to 0.2 mmol/L, and the tissue was stirred for an additional 35 minutes in protease-free solution until rod-shaped single atrial myocytes were released. The cell suspension was centrifuged, and cardiomyocytes were resuspended in a storage solution (20 mmol/L KCl, 10 mmol/L KH_2PO_4 , 10 mmol/L

glucose, 70 mmol/L K glutamate, 10 mmol/L β -hydroxybutyrate, 10 mmol/L taurine, 10 mmol/L ethylene glycol tetraacetic acid, 1% albumin). Patch clamp measurements were performed in whole cell configuration at room temperature (21–25°C) using either a RK-400 (Bio-Logic SAS, Seyssinet-Pariset, France) or an Axopatch 200B amplifier (Molecular Devices LLC, San José, CA). Glass pipettes were pulled from borosilicate glass (1B120F-4; World Precision Instruments, Berlin, Germany). After back-filling with internal solution (60 mmol/L KCl, 65 mmol/L K glutamate, 3 mmol/L K_2 ATP, 0.2 mmol/L Na_2 GTP, 2 mmol/L $MgCl_2$, 5 mmol/L ethylene glycol tetraacetic acid, 5 mmol/L 4-(2-hydroxyethyl)piperazine-1-ethanesulfonic acid (HEPES), pH adjusted to 7.2 with potassium hydroxide) tip resistances ranged from 3 to 4 M Ω . Cardiomyocytes subjected to background potassium current recordings were constantly superfused with an extracellular solution (140 mmol/L NaCl, 5.4 mmol/L KCl, 1 mmol/L $MgCl_2$, 1 mmol/L $CaCl_2$, 0.33 mmol/L NaH_2PO_4 , 5 mmol/L HEPES, 10 μ mol/L tetrodotoxin, 1 μ mol/L nifedipine, and 10 mmol/L glucose, pH adjusted to 7.4 with NaOH). Seal resistances yielded 4 to 8 G Ω . Series resistance and cell capacitance were compensated. Data were not corrected for liquid junction potentials. Membrane currents were evoked by application of voltage steps between –60 and +60 mV in 10-mV increments (duration, 400 ms; holding potential, –50 mV) as depicted. Patch pipettes for cardiac action potential recordings were filled with 134 mmol/L K gluconate, 6 mmol/L NaCl, 1.2 mmol/L $MgCl_2$, 1 mmol/L MgATP, 10 mmol/L HEPES, pH adjusted to 7.2 with potassium hydroxide. Extracellular Tyrode's solution was composed of 137 mmol/L NaCl, 5.4 mmol/L KCl, 2 mmol/L $CaCl_2$, 1 mmol/L $MgSO_4$, 10 mmol/L glucose and 10 mmol/L HEPES, pH 7.3 with NaOH. Action potentials were elicited in current clamp mode with a holding current of –40 pA by injection of brief current pulses (2 ms, 1 nA) at 0.2 Hz stimulation rate.

Molecular Biology and *Xenopus* Oocyte Electrophysiology

Plasmid constructs containing cDNA encoding human TASK-1 (GenBank accession no. NM_002246) cloned in the expression vector pRAT were kindly provided by Steve Goldstein (Brandeis University, Waltham, MA). The pMAX-pTASK-1 construct, encoding for porcine TASK-1 (KF182337.1), was cloned from porcine cardiac cDNA, as described earlier.¹⁴ In vitro synthesis of copy RNA was performed using the mMESAGE mMACHINE T7 Transcription Kit (Thermo Fisher Scientific, Waltham, MA) according to the manufacturer's instructions, as described earlier.²⁰ Integrity of transcripts was assessed via agarose gel electrophoresis and

concentration was determined by spectrophotometry (ND-2000, Thermo Fisher Scientific). For oocyte preparation, ovarian lobes were surgically removed in aseptic techniques from female *Xenopus laevis* frogs (Xenopus Express, Le Bourg, France), anesthetized with tricaine solution (1 g/L, pH 7.5, 15°C). Frogs were kept in specific pathogen-free aquarium facilities with continuous water flow (Aqua Schwarz GmbH, Göttingen, Germany) at a housing density according to directive 2010/63/EU. Water temperature was kept at 18°C and room lighting had a light/dark cycle of 12/12 h. Frogs were fed daily with food extrudate 3590.ES.F10 (Kliba Nafag, Kaiseraugst, Switzerland) and environmental enrichment was provided with huts and polyvinyl chloride pipes. No more than 4 operations were performed on 1 individual frog.

After collagenase treatment, stages V and VI defolliculated oocytes were manually selected under a stereo microscope and injected with 1.5 to 25 ng of cRNA. Two-electrode voltage clamp recordings of macroscopic currents were performed, as reported earlier.¹⁸ In brief, measurements were performed 1 to 4 days after cRNA injection using a Warner OC-725C amplifier (Warner Instruments, Hamden, CT) and pCLAMP9 (Axon Instruments, Foster City, CA) software for data acquisition. Electrodes were pulled from borosilicate glass (GB 100F-10, Science Products, Hofheim, Germany) using a Flaming/Brown P-87 micropipette puller (Sutter Instruments, Novato, CA). After back-filling with 3 M of KCl, tip resistances yielded 1 to 2.5 m Ω . All recordings were performed at room temperature (20–22°C) in a standard physiological extracellular solution, consisting of: 96 mmol/L NaCl, 4 mmol/L KCl, 1.1 mmol/L $CaCl_2$, 1 mmol/L $MgCl_2$, and 5 mmol/L HEPES (pH 7.4). TASK-1 currents were evoked by application of 500-ms test pulses from –80 to +60 mV in 20-mV increments from a holding potential of –80 mV. Leak currents were not subtracted.

Tissue Handling and Quantitative Real-Time Polymerase Chain Reaction Expression Analysis

Tissue samples of right or left atrial appendages were obtained from patients undergoing open heart surgery for coronary artery bypass grafting or valve repair or replacement. Left ventricular tissue samples were acquired from patients with ischemic or dilated cardiomyopathy during left ventricular assist device implantation. Porcine hearts were extracted after intracardiac injection of KCl in deep anesthesia, rinsed in phosphate buffered saline and quickly dissected. Tissue samples were flash-frozen in liquid nitrogen and stored at –80°C, and RNA isolation was performed using TRIzol Reagent (Thermo Fisher Scientific) according

to the manufacturer's protocol. RNA concentration was quantified via nanodrop spectrophotometry, and synthesis of single-stranded cDNA was carried out using the Maxima First Strand cDNA Synthesis Kit (Thermo Fisher Scientific) with 3 μg of total RNA per 20 μL reaction. Quantitative real-time polymerase chain reaction was carried out as reported.²¹ In brief, 10 μL per reaction, consisting of 0.5 μL cDNA, 5 μL TaqMan Fast Universal Master Mix (Thermo Fisher Scientific), and 0.5 μL 6-carboxyfluorescein (FAM)-labeled TaqMan probes and primers (TaqMan Gene Expression Assays; Thermo Fisher Scientific) were analyzed using the StepOnePlus (Applied Biosystems, Foster City, CA) PCR system. *Importin 8* (*IPO8*, HS 00183533_m1; Thermo Fisher, Darmstadt, Germany) as well as *beta-actin* (*ACTB*, Ss03376081_u1; Thermo Fisher Scientific) housekeeping genes were used for normalization of signals of *KCNK3* mRNA encoding TASK-1 (Hs00605529_m1; Thermo Fisher Scientific). All quantitative real-time polymerase chain reactions were performed as triplicates and control experiments in the absence of cDNA were included. Means of triplicates were used for calculating $2^{-\Delta\text{Ct}}$, the ratio of mRNA expression versus respective housekeeping genes.

Homology Model and Docking Simulation

Three-dimensional open-state structure models of pTASK-1 channels were calculated on the basis of the crystal structure of hTREK-1 (PDB ID: 6CQ8)²² using the SWISS-MODEL platform.^{23–26} For visualization of A293 in the pTASK-1 central cavity, molecular docking calculations were performed using AutoDock Vina.²⁷ Polar hydrogens and Kollmann charges were added using AutoDockTools 1.5.6.²⁸ The cubic grid box had an axial length of 35 Å and was centered on the intracellular central channel cavity, where the binding site of A293 in human TASK-1 had been identified earlier.¹⁸ Docking simulations were performed with potassium ions in positions S1 and S3 within the selectivity filter of TASK-1. Three-dimensional visualizations of in silico simulations and dockings were generated with PyMOL 1.8 (PyMOL Molecular Graphics System, Schrödinger, LLC, New York, NY).

Computational Simulations

The computational description of the influence of TASK-1 channel inhibition on atrial reentry behavior is based on the Courtemanche–Ramirez–Nattel model of human atrial electrophysiology²⁹ in conjunction with a description of the $\text{K}_{2\text{P}}$ channel.¹⁰ To avoid long-term drift of the Courtemanche–Ramirez–Nattel model,³⁰ concentrations of intracellular sodium ($[\text{Na}^+]_i$) and potassium ($[\text{K}^+]_i$) were kept constant. The channel conductivity of I_{K1} and I_{Kur} were adjusted (in line with

Schmidt et al¹⁰) to represent the measured atrial effective refractory periods (AERPs) at the basic cycle length (BCL) of 300, 400, and 500 ms (see Results) including A293: g_{K1} and g_{Kur} were increased by 62.5% and 50%, respectively. The parameters of the TASK-1 model were then adjusted to reconstruct the measured AERPs without A293 at the BCLs: the TASK-1 conductivity for AF cells was set to 0.0035 nS/pF to simulate the state without drug bound to the channel. For all simulations, the CARPentry monodomain software was used with a time step of 10 microseconds using the Crank–Nicolson method in conjunction with mass lumping.³¹ To predict the A293 dose-dependent prolongation of APD in a single-cell environment, we used the Hill equation with an IC_{50} value of 100 nmol/L¹⁶ and a Hill coefficient of 1. Dose-response curves were calculated for a BCL of 200, 300, 500, and 1000 ms. The APD at 90% repolarization (APD_{90}) of the 100th beat was evaluated to allow adaptation of the simulated system to BCL and drug dose.

The effect of TASK-1 channel blockade on atrial arrhythmia is shown in a simplified left atrial geometry.³² This consists of a 2-dimensional sphere surface with a diameter of a standard human left atrium (5 cm) and 5 orifices representing the 4 pulmonary veins as well as the mitral valve. The model has an average edge length of the underlying tetrahedra of 0.5 mm and is homogeneous and isotropic to keep it as simple as possible to neglect interindividual differences. In all simulations, the cell states were adjusted to a BCL of 300 ms according to single-cell results after 50 stimulations. Additionally, on the basis of 1-phase singularity (center point of a rotor), the cell states were adjusted to start the simulation with 1 rotor at a given location.^{32,33} The initial rotor was simulated for 10 seconds with different tissue conductivities and thus conduction velocities. Additional 5 seconds for each conductivity were calculated for both blocked and unblocked TASK-1 channels. We investigated in which range of tissue conductivities A293 was able to eliminate the rotor.

Statistical Analysis

PCLAMP 10 (Axon Instruments, Foster City, CA), Origin 8 (OriginLab, Northampton, MA), Prism 8 (GraphPad, La Jolla, CA), and Excel (Microsoft, Redmond, WA) software was used for data acquisition and analysis. Data are expressed as mean \pm SEM. Nonparametric Kruskal–Wallis tests, Mann–Whitney tests, or Wilcoxon matched-pairs tests were applied to compare the statistical significance in cases of small sample sizes where the assumption of normality would be difficult to assess. If the hypothesis of equal means could be rejected at the 0.05 level, pairwise comparisons of groups were made and the probability values were adjusted for

multiple comparisons using the Bonferroni correction. In situations with sample sizes of <5, Student *t* tests were used instead of nonparametric tests and normal distribution was assessed with Anderson–Darling tests.

RESULTS

Homology of Human and Porcine TASK-1 Orthologs and Atrial Specific Tissue Expression

The pig represents an established and clinically relevant large animal model for AF. Major anatomic and physiological analogies to humans constitute specific advantages of pigs compared with rodents, zebrafish, or other commonly used small animal models. To assess whether the pig would be suitable for studying the role of TASK-1 channels in atrial electrophysiology, we performed structural and functional comparisons of porcine and human TASK-1 channels. Cloning and functional characterization of the porcine TASK-1 orthologs was described earlier.¹⁴ Amino acid sequence alignments of pTASK-1 and hTASK-1 showed 96.7% conservation at the protein level (Figure 1A). While the transmembrane regions were found to be highly conserved between hTASK-1 and pTASK-1, minor differences were found for the N- and C-termini of the channel protein. One single amino acid substitution (H180T) is located within the third transmembrane domain (M3) at a distance of 20 amino acid residues to the selectivity filter motif of the second pore-forming loop (Figure 1A).

In the human heart, TASK-1 channels are specifically expressed in the atria, whereas ventricular TASK-1 expression levels are virtually negligible.^{10,12,13} Real-time quantitative real-time polymerase chain reaction experiments showed that subcompartment-specific patterns of *KCNK3* mRNA levels in the porcine heart are similar to expression patterns in the human heart. Abundant expression was observed in the left atrial appendages

as well as in the right atrial appendages, while expression in left ventricular tissue was low (Figure 1B).

Inhibition of Heterologously Expressed TASK-1 Potassium Channels by A293

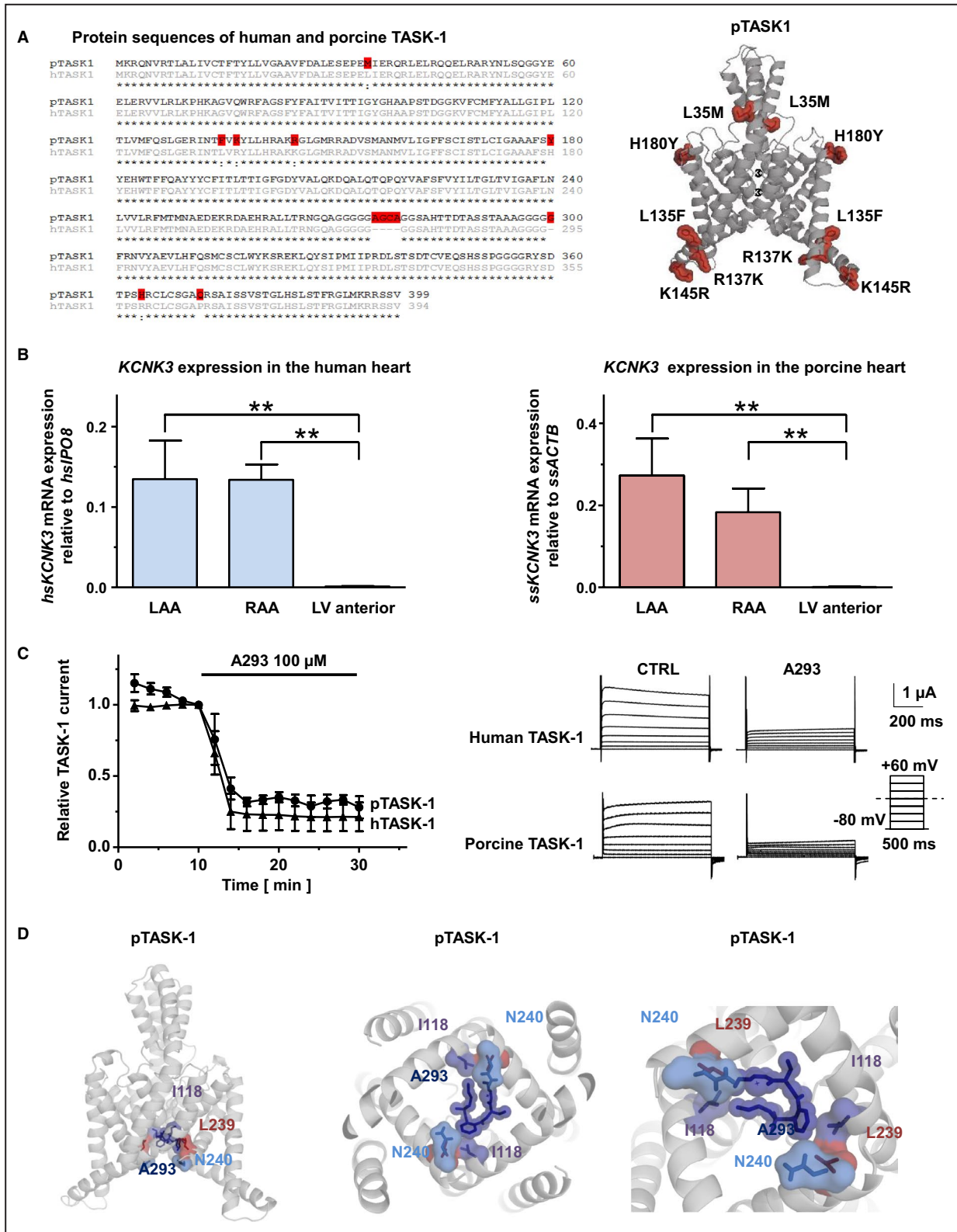
Human and porcine TASK-1 channel subunits that were heterologously expressed in *Xenopus laevis* oocytes gave rise to comparable macroscopic currents (Figure 1C). Forty-eight hours after injection of RNA encoding either human or porcine TASK-1 orthologs, *Xenopus laevis* oocytes were subjected to two-electrode voltage clamp measurements. Outward potassium currents were elicited by application of the pulse step protocol depicted in Figure 1C. Depolarizing test pulses of 500 ms were applied in +20-mV increments from a holding potential of –80 mV to +60 mV at a frequency of 0.2 Hz. The measurements were repeated every 2 minutes. Upon administration of the high-affinity TASK-1 inhibitor A293 (100 μmol/L) into the extracellular solution, a rapid current decline to 21.3±8.7% (n=3, hTASK-1) and 28.0±6.8% (n=3, pTASK-1) of the control currents was observed (Figure 1C). These findings suggest that the structural similarities between porcine and human TASK-1 channels are linked to comparable pharmacologic characteristics. Next, we used in silico docking simulations to predict how the A293 molecule binds to the inner pore of the pTASK-1 channels and thereby occludes the passage of potassium ions through the channel selectivity filter. Figure 1D visualizes the simulated docking of A293 to hTASK-1. The docking site is near the pore-lining amino acids L239 and N240. Recently, it was experimentally shown that these amino acids are indeed part of the molecular binding site of A293 at hTASK-1.¹⁸

Comparison of TASK-1 Currents in Porcine and Human Atrial Cardiomyocytes

To further assess whether similar functional properties and cardiac expression patterns of the human

Figure 1. Structural and functional comparison of human and porcine TASK-1 channels.

A, Left panel: Amino acid alignments of pTASK-1 and hTASK-1 show high similarity between human and porcine orthologs at the protein level. Differences are highlighted in red (*, conserved amino acids; :, amino acid substitutions by residues with similar properties). **Right panel:** Differences between human and porcine TASK-1 are highlighted in a 3-dimensional structure homology model of pTASK-1 in red color. C-termini were truncated because of lack of template sequences. **B,** Real-time quantitative polymerase chain reaction experiments revealed similar atrial specific TASK-1 expression patterns in human and porcine cardiac tissue. *KCNK3* mRNA expression is presented relative to the housekeeping genes importin 8 (*IPO8*) or β-actin (*ACTB*) in left atrial appendages (LAA), right atrial appendages (RAA) and the anterior wall of the left ventricle (LV) (n=5). **C,** Cloned human and porcine TASK-1 ion channel subunits, heterologously expressed in *Xenopus laevis* oocytes, are inhibited by A293 (100 μmol/L) to a similar extent. Currents were recorded using two-electrode voltage clamp technique measurements after application of the depicted pulse protocol. Quantification was performed at the end of the +20 mV pulse (n=3 cells). Representative current traces of hTASK-1 and pTASK-1 before (Control) and after application of A293 (100 μmol/L, 30 min) are indicated on the right side. Scalebars are given as inserts. **D,** In silico docking simulation of A293 in the inner channel pore of a pTASK-1 homology model and magnified excerpts illustrate the interactions of A293 with the pore lining amino acids I118, L239 and N240. Data are presented as mean±SEM. ***P*<0.01 in Mann–Whitney tests. TASK-1 indicates TWIK-related acid-sensitive K⁺ channel.



and porcine TASK-1 channels result in comparable TASK-1 currents at the single-cell level, we subjected isolated atrial human and porcine cardiomyocytes to patch clamp measurements. The human atrial cardiomyocytes were derived from patients with sinus

rhythm without a prior history of AF episodes and without relevant left ventricular dysfunction.

Background potassium currents were evoked by the application of voltage steps between -60 and +60 mV in 10-mV increments from a holding potential

of -50 mV (Figure 2A and 2B). The TASK-1 currents were isolated by application of A293 (200 nmol/L) as reported previously.^{10,11} The current-voltage relationships of the background potassium currents before and after administration of A293 are depicted in Figure 2C and 2D (human cardiomyocytes: $n=16$ cells obtained from $N=6$ individuals; porcine cardiomyocytes: $n/N=8/4$). While human atrial cardiomyocytes displayed slightly higher background potassium current densities at the baseline level, administration of A293 (200 nmol/L) resulted in comparable current inhibition (Figure 2E). The calculated A293-sensitive K^+ current densities were activated at potentials >-20 mV and showed Goldman-Hodgkin-Katz rectification, which is typical for K_{2P} channels (Figure 2F). In porcine cardiomyocytes, the TASK-1 current density quantified at $+40$ mV reached 68% of the currents obtained from isolated human atrial cardiomyocytes (human: $n/N=16/6$; porcine: $n/N=8/4$, Figure 2G). Representative micrographs of isolated human and porcine atrial cardiomyocytes are presented in Figure 2H.

Effects of TASK-1 Current Inhibition on the APDs of Porcine and Human Atrial Cardiomyocytes

Atrial APs were studied under current-clamp conditions in human and porcine atrial cardiomyocytes, and the TASK-1 currents were again isolated via application of A293 (Figure 2I and 2J). In human atrial cardiomyocytes, administration of A293 (200 nmol/L) prolonged the APD at 50% repolarization (APD_{50}) by 6% and the APD_{90} by 18% ($n/N=9/5$; $p_{APD50}=0.0087$; $p_{APD90}=0.009$; Wilcoxon matched-pairs test), while in porcine cardiomyocytes, prolongations of the APD_{50} by 19% and the APD_{90} by 24% were observed ($n/N=5/4$; $p_{APD50}=0.81$; $p_{APD90}=0.63$; Wilcoxon matched-pairs test; Figure 2K and 2L).

Taken together, the functional similarities between the porcine and human TASK-1 channels and the comparable cardiac expression patterns indicate that the pig represents an adequate model

for studying the role of TASK-1 currents in cardiac electrophysiology.

Effects of A293 on Surface ECG Parameters

To assess the effects of TASK-1 inhibition by A293 on cardiac electrophysiology, we recorded the surface ECGs from anesthetized pigs before and after application of A293. Five healthy male German landrace pigs with a body weight of 30 to 45 kg were anesthetized, and 1 mg/kg body weight of A293 was administered as an intravenous short infusion. No significant differences in surface ECG parameters upon A293 treatment were observed (Figure 3).

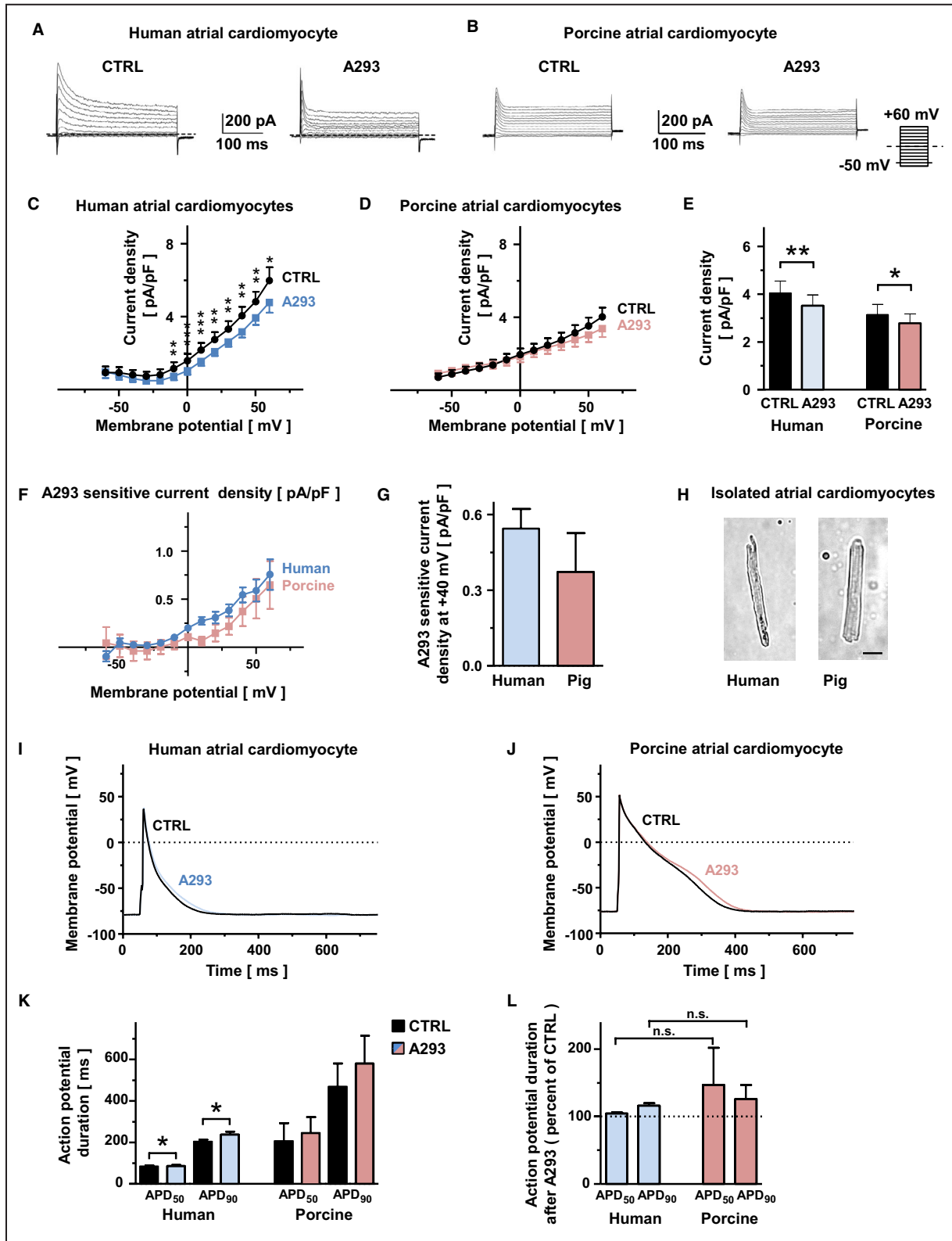
TASK-1 Inhibition by A293 Selectively Prolongs the Atrial Effective Refractory Periods

AERPs were assessed through invasive electrophysiological studies. AERPs, measured at different BCLs, were significantly prolonged upon TASK-1 inhibition by A293 (Figure 4A through 4H). Vascular access after surgical jugular vein preparation and fluoroscopic placement of quadripolar diagnostic catheters is visualized in Figure 4A and 4B. AERP measured at a BCL of 500 ms ($AERP_{500}$) was shifted by 20 ms from 200 ± 4.1 ms under control conditions to 220 ± 4.1 ms after intravenous infusion of A293 ($P=0.016$; $n=4$ pigs; Figure 4C). $AERP_{400}$ was prolonged by 22.5 ms from 175 ± 9.6 ms to 197.5 ± 9.5 ms after TASK-1 inhibition by ($P=0.037$; Student *t* test; $n=4$ pigs; Figure 4E), and $AERP_{300}$ was prolonged by 17.5 ms from 155 ± 13.2 ms to 172.5 ± 13.1 ms under A293 treatment ($P=0.006$; $n=4$ pigs; Figure 4G).

In addition, the ventricular effective refractory periods at different BCLs remained unchanged after intravenous A293 treatment (Figure 4D and 4F), demonstrating atrial-specific class III antiarrhythmic effects of A293 (Figure 4H). Furthermore, no proarrhythmic effects under A293 treatment were observed while performing programmed ventricular stimulation.

Figure 2. Comparison of TASK-1 currents in human and porcine atrial cardiomyocytes.

A and **B**, Representative background potassium currents, recorded from isolated human (**A**) or porcine (**B**) cardiomyocytes under control conditions (CTRL) and after administration of the high affinity TASK-1 channel inhibitor A293, 200 nmol/L (A293). Dashed lines represent zero current level. The pulse protocol is depicted at the right bottom corner of panel (**B**). **C** and **D**, Corresponding mean step current densities are displayed as a function of the respective test potentials for human (**C**) and porcine (**D**) cardiomyocytes (human cardiomyocytes: $n=16$ cells obtained from $N=6$ individuals; porcine cardiomyocytes: $n/N=8/4$). **E**, Comparison of mean current density, quantified at $+40$ mV membrane potential. **F**, Current-voltage relationships of mean A293-sensitive current density are displayed for human (blue) and porcine (red) atrial cardiomyocytes (human: $n/N=16/6$, porcine: $n/N=8/4$). **G**, Comparison of mean A293-sensitive current density measured at a membrane potential of $+40$ mV (human: $n/N=16/6$, porcine: $n/N=8/4$). **H**, Micrographs of representative isolated human (left) and porcine (right) atrial cardiomyocytes. The scalebar (bottom right) depicts 20 μ m. **I** and **J**, Representative action potentials (APs) recorded at 0.2 Hz in the absence or presence of A293 (200 nmol/L) are shown for isolated human (**I**) and porcine (**J**) atrial cardiomyocytes. **K**, Corresponding mean AP durations at 50% of repolarization (APD_{50}) and 90% repolarization (APD_{90}) at baseline and after A293 application (human: $n/N=9/5$, porcine: $n/N=5/4$). **L**, Mean relative APD_{50} and APD_{90} values after TASK-1 inhibition with 200 nmol/L A293 (human: $n/N=9/5$, porcine: $n/N=5/4$). Data are expressed as mean \pm SEM. * $P<0.05$, ** $P<0.01$, *** $P<0.001$ vs CTRL for Mann-Whitney tests or Wilcoxon matched pairs tests.



A293 Facilitates Cardioversion in a Porcine Model of Acute Paroxysmal AF

A porcine model of acute paroxysmal AF was employed to evaluate whether A293-induced AERP prolongation

has antiarrhythmic effects. Following jugular vein preparation, diagnostic electrophysiology catheters were placed under fluoroscopic guidance in the upper right atrium and at the right ventricular apex position. AF was induced via right atrial burst pacing (10 V, 150–50-ms

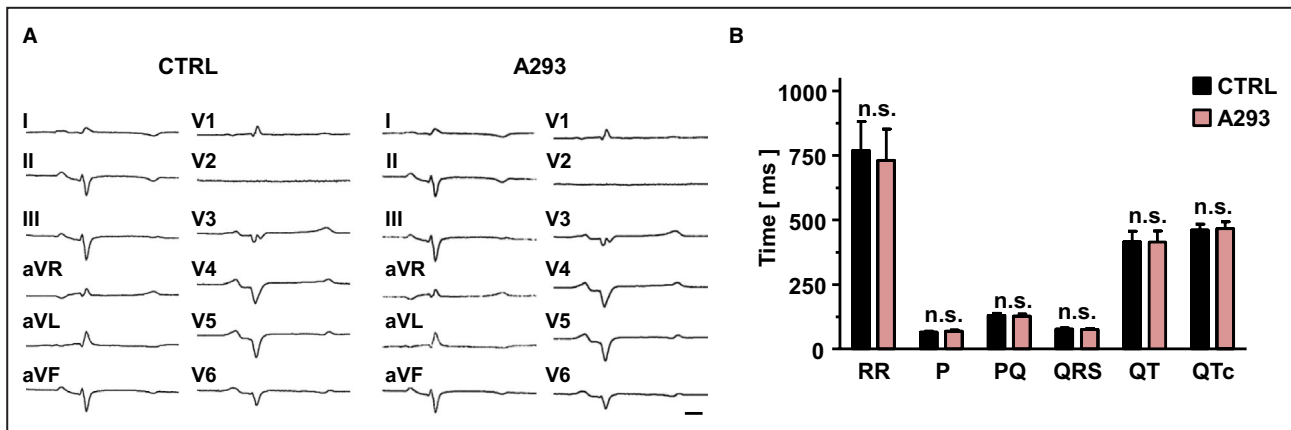


Figure 3. Administration of A293 does not alter surface ECG parameters of healthy control pigs.

A, Representative surface ECG recordings of an anesthetized pig under baseline conditions (left) and 20 min after *i.v.* administration of A293 at 1 mg/kg body weight (right). The scale bar, provided as insert (bottom right), indicates 100 ms. **B**, RR intervals, P wave durations, PQ intervals, QRS durations, QT intervals, and QTc intervals of pigs treated with A293 display no significant differences to baseline conditions ($n=5$ pigs; n.s., no statistically significant difference in Wilcoxon matched-pairs tests). aVF indicates augmented Vector foot; aVL, augmented Vector left; and aVR, augmented Vector right.

cycle length, duration of 2–8 seconds). Upon induction of AF, the atrial rhythm was monitored for 5 minutes to confirm the stability of the AF episode. Pigs that remained in AF after this 5-minute period were subjected to treatment with either A293 or the vehicle controls (Figure 5A). In the vehicle control group, only 2 of 8 spontaneous conversions were observed ($n=8$ pigs). In contrast, a cardioversion rate of 100% ($n=5$ pigs) was documented after intravenous application of A293 (Figure 5B). Pharmacologic cardioversion with A293 yielded cardioversion times of 177 ± 63 seconds, differing significantly from that of the control group ($P=0.0034$, Kruskal–Wallis test) as visualized in Figure 5C.

Computational Modeling of the A293 Effects on Atrial Electrophysiology in a Single-Cell and a Tissue Model

To assess the causal role of TASK-1 current inhibition in the termination of AF, we performed computational modeling at the single-cell and 2-dimensional tissue levels. Therefore, the Courtemanche–Ramirez–Nattel model of human atrial electrophysiology²⁹ was extended by TASK-1.¹⁰ A human model of atrial electrophysiology was chosen, first, because no porcine electrophysiological model is available and, second, because it integrates a translational aspect into this study. In Figure 6A, simulated APs of the atrial cardiomyocyte model are depicted at four BCLs without the addition of A293 (solid line) and with a full block of TASK-1 channels by A293 (dashed line). The model was adjusted to reproduce the prolongation of the AERP due to A293 at 3 different BCLs (Figure 6A): from 157 to 173.6 ms for a BCL of 300 ms; from

173.7 to 194.1 ms for a BCL of 400 ms; and from 185.9 to 209.1 ms for a BCL of 500 ms. The other BCL-dependent prolongations of the action potential duration (APD) were predicted by the model. At a BCL of 200 ms, the model predicted a drug-induced prolongation of the APD by 12.6 ms (from 136 to 148.6 ms, purple line in Figure 6A). At BCLs of 1000 ms, the APD was prolonged by 27.1 ms (from 208.6 to 235.7 ms, red line in Figure 6A). In Figure 6B, the APD_{90} is visualized depending on the concentration of A293 (IC_{50} of 100 nm) at 4 different BCLs. Boxplots depicting APD_{90} values obtained from patch clamp experiments performed on human atrial cardiomyocytes (Figure 2K and 2L) under control conditions and after application of 200 nmol/L A293 are compared with our computational model data. Finally, the predicted relative change in APD_{90} is visualized as a function of the A293 concentration in Figure 6C. Notably, the highest level of relative APD prolongation by A293 was observed at high BCLs (Figure 6C).

Finally, the antiarrhythmic potential of TASK-1 current inhibition was investigated in multicellular tissue simulations. A simplified left atrial geometry consisting of a 2-dimensional spherical surface with a diameter of 5 cm and 5 orifices representing the 4 pulmonary veins and the mitral valve (see Figure 6D, black spheres) was employed. The tissue simulation was started with 1 rotational activity and in the absence of TASK-1 current inhibition by A293. The initial rotor was simulated for 10 seconds with different tissue conductivities, resulting in differing conduction velocities. Subsequently, 5 seconds was simulated for each conductivity value, either in the presence or absence of TASK-1 current inhibition by A293. We investigated the range in which

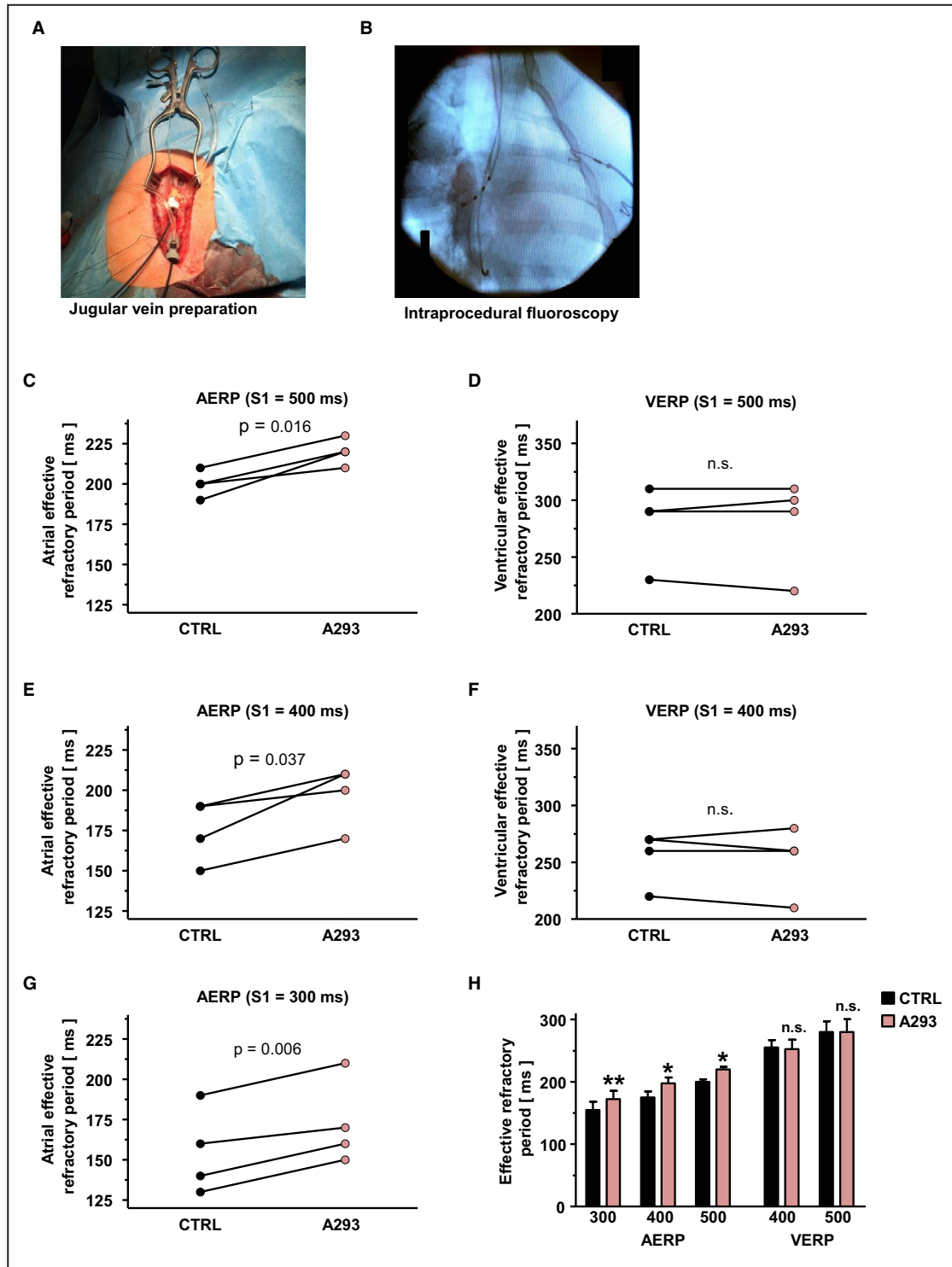


Figure 4. A293 selectively prolongs atrial effective refractory periods (AERPs).

A, Perioperative view after surgical jugular vein preparation and placement of 2 introducer sheaths into the right internal jugular vein. **B**, Intraoperative fluoroscopy showing a quadripolar diagnostic catheter in the high right atrium position and another quadripolar diagnostic catheter in the right ventricular apex. **C** through **G**, Atrial (AERPs) as well as ventricular effective refractory periods (VERPs), measured at an S1 cycle length of 500 ms (**C** and **D**), 400 ms (**E** and **F**), or 300 ms (**G**) under control conditions or 20 minutes after intravenous administration of A293 at 1 mg/kg body weight in anesthetized pigs (n=4 pigs each; P values are indicated as inserts). **H**, Application of A293 resulted in a significant AERP-prolongation whereas VERPs remained unchanged. Data are presented as mean±SEM. *P<0.05; **P<0.01 for Student t tests.

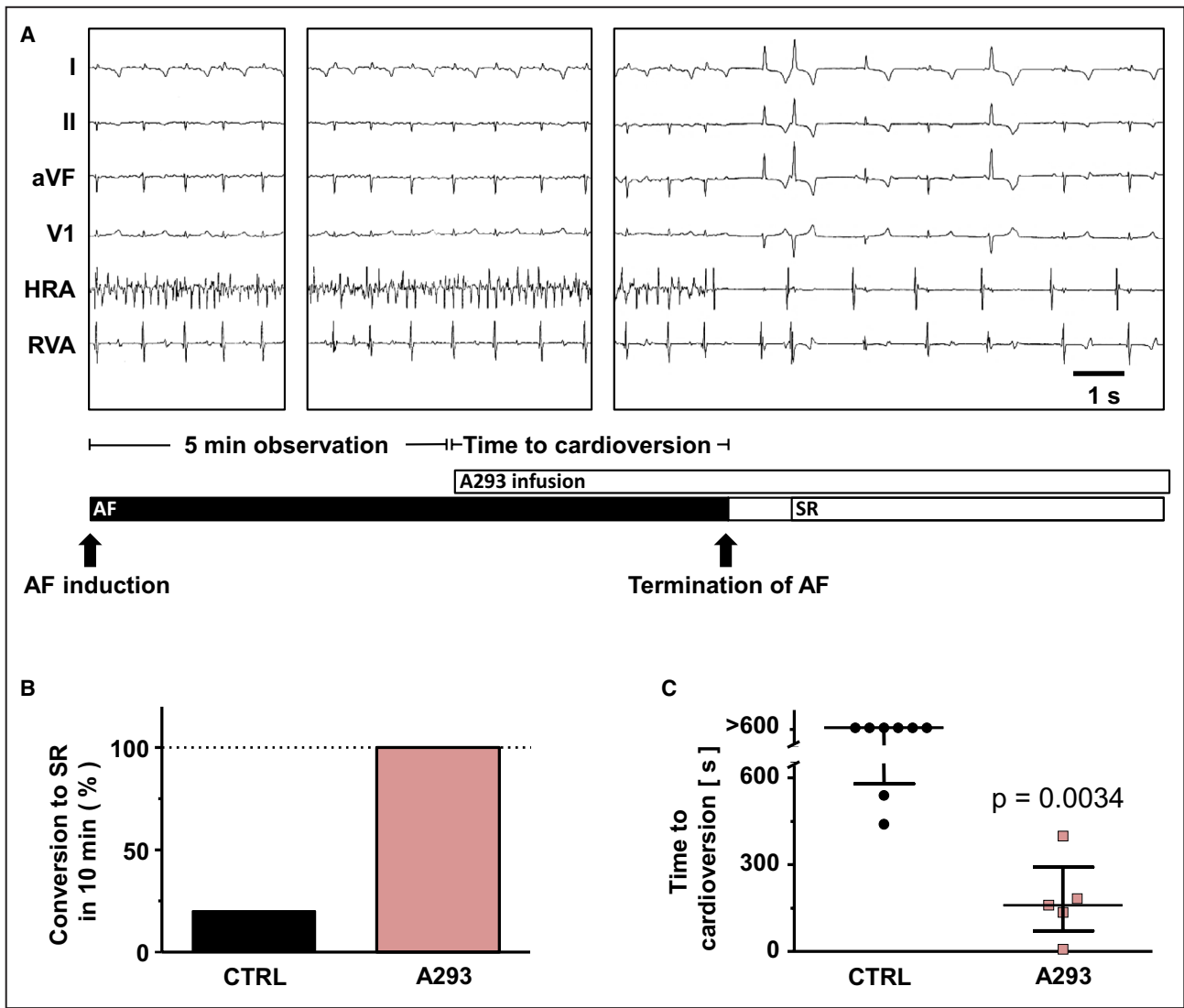


Figure 5. A293 facilitates cardioversion in a porcine model of paroxysmal atrial fibrillation (AF). **A**, After induction of AF by right atrial burst-stimulation in anesthetized pigs, the atrial rhythm was monitored for 5 minutes. When AF persisted over this 5-minute period, A293 or the respective solvent control was administered. Cardioversion was monitored up to 10 minutes after drug administration. **B**, Percentage of cardioversions to sinus rhythm (SR) during the 10-minute observation interval in the solvent control (Control) and the A293 treatment group (A293). **C**, Time to conversion to SR in the solvent control (Control) and the A293 treatment group (data are presented as medians; whiskers indicate interquartile ranges for n=5 to 8 individual experiments; P value was obtained from Kruskal–Wallis test). AF indicates atrial fibrillation; aVF indicates the surface ECG lead aVF; HRA, intracardiac catheter at the high right atrium; and RVA, intracardiac catheter at the right ventricular apex.

tissue conductivities A293 could eliminate the rotor. The results of the tissue simulations at a conductivity of 1.0 S/m (corresponding to a plane wave conduction velocity of 80 cm/sec at a BCL of 1000 ms) are shown in Figure 6D through 6F (Videos S1 through S3). The highest conductivity value at which persistent reentry could be stopped by A293 was at 1.2 S/m (equal to 90 cm/sec). Larger conductivity values led to termination even without the drug. The model predicted that the lowest conductivity at which the drug stopped the arrhythmia was 0.95 S/m (resulting in a plane wave conduction velocity of 77 cm/s at a BCL of 1000 ms). For lower conductivity, the model persisted always in reentry.

Thus, model simulations support the antiarrhythmic effects of TASK-1 inhibition. Further, multicellular tissue modeling predicted that the antiarrhythmic effect of TASK-1 inhibition by A293 was strongly dependent on the tissue conductivity and the resulting conduction velocity.

DISCUSSION

Current antiarrhythmic AF treatment is limited by sub-optimal effectiveness and often causes adverse side effects.^{1,3} The development of more effective therapies

is needed to increase quality of life by reducing the symptoms and hospitalizations associated with AF. Atrial selectivity is an important aim in the development of novel antiarrhythmic approaches.³⁴ In the human heart, TASK-1 channels are predominantly expressed in the atria and might therefore represent a promising novel target for atrial-specific AF therapy.^{10,12}

Protein sequences of human and porcine TASK-1 ion channel subunits share a high degree of homology. The pharmacologic sensitivity of porcine and human TASK-1 currents to A293 was similar. In human as well as porcine myocardial tissue samples, TASK-1 mRNA was primarily detected in the atria. The pig therefore represents an adequate model to study the cardiac role of TASK-1. In contrast, in rodents, TASK-1 expression is not confined to the atria, and AF-related TASK-1 remodeling differed from the effects observed in the tissue samples of AF patients.²¹ Finally, patch clamp recordings performed on native isolated atrial cardiomyocytes confirmed comparable TASK-1 current densities in humans and pigs with a nonsignificant trend toward higher TASK-1 currents in patient samples. It remains speculative whether this slight elevation of the atrial TASK-1 currents may be linked to the underlying atrial cardiomyopathy, as patients that underwent open heart surgery due to ischemic or valvular heart disease were compared with young and healthy pigs. Of note, human tissue samples were taken from patients with sinus rhythm without documentation of AF in their prior medical history and without relevant left ventricular dysfunction. Despite differences in APD under control conditions, TASK-1 current inhibition resulted in a similar prolongation of human and pig atrial cardiomyocyte APD. Our preclinical proof-of-concept trial in pigs confirmed that pharmacological TASK-1 inhibition by A293 prolongs atrial refractoriness with no effects on ventricular repolarization. ECG analyses further supported the absence of side effects on ventricular electrophysiology. Based on a clinically relevant large animal model, we showed that blockade of atrial TASK-1 currents exerts class III antiarrhythmic effects *in vivo*, resulting in acute cardioversion of paroxysmal AF episodes. This study is, to our knowledge, the first report demonstrating the potential of pharmacological TASK-1 inhibition for acute cardioversion.

In silico model simulations mechanistically reproduced the antiarrhythmic effect of TASK-1 inhibition in a single-cell model of human atrial cardiomyocytes. Both, effects of A293 on APD₉₀ values measured in patch clamp experiments on human atrial cardiomyocytes and antiarrhythmic effects as observed in our large animal experiments could be recapitulated *in silico*. This model could be used to create predictions for a wider range of experimental conditions and therefore provides a platform for future mechanistic and interventional studies. Of note, the strongest effects of APD

prolongation by A293 were predicted for the longest BCLs, implying that tissue with A293 has a decreased chance to develop arrhythmia (Figure 6C).

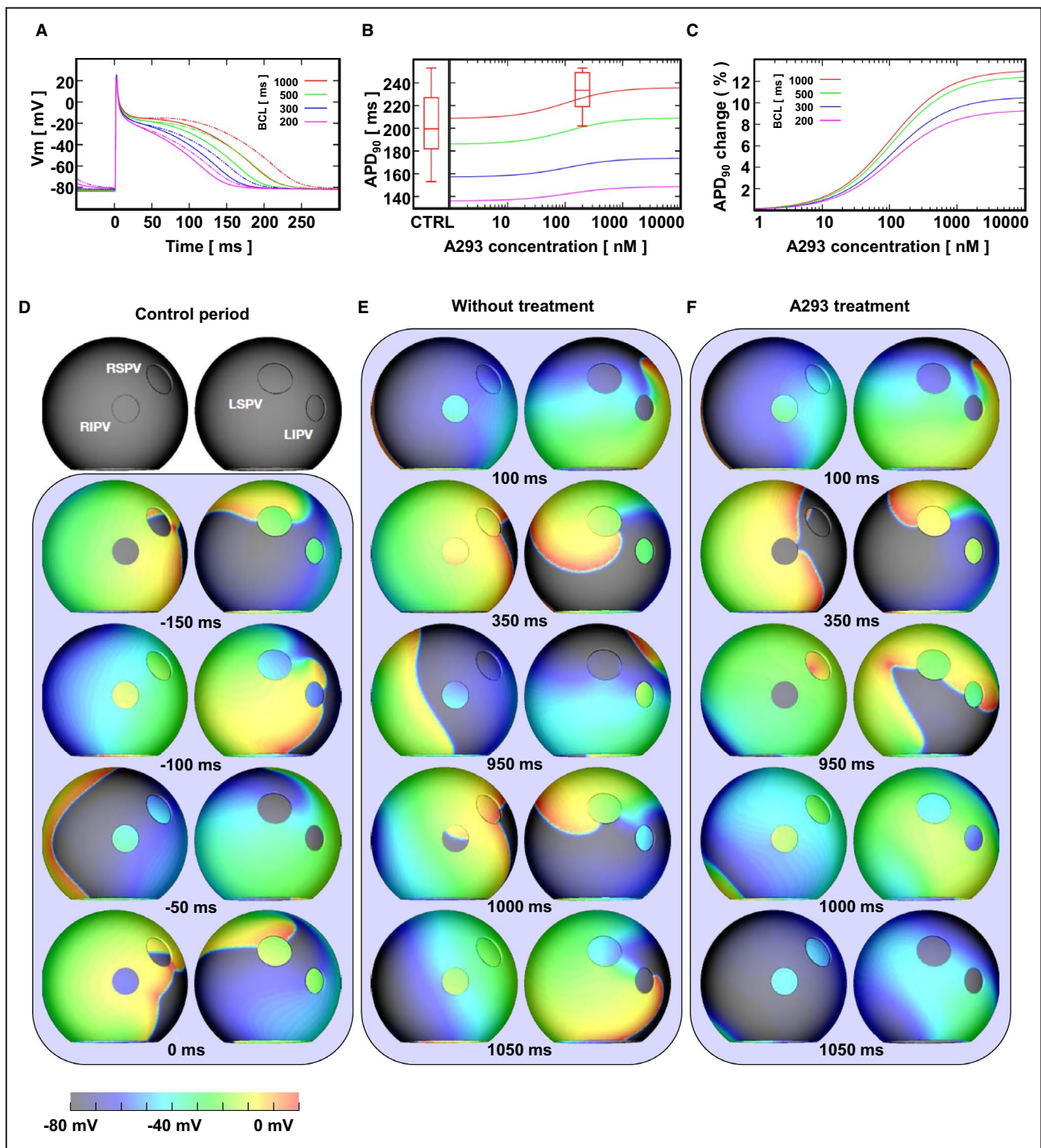
A293 was initially developed as a K_v1.5 channel inhibitor by Sanofi Aventis. This drug later was shown to exhibit a 42-fold higher affinity for TASK-1 channels than K_v1.5 channels.^{16–18} Some proprietary data of Sanofi Aventis were published by Wirth et al in 2007³⁵: In a small series of large animal experiments, A293 (there known as AVE1231) prolonged AERPs.^{17,35} Although a different route of delivery (enteral application via gastric tube) and another stimulation site (left atrium instead of right atrium) were used, Wirth et al³⁵ reported AERP prolongations at different BCLs by 19 to 20.8 ms, similar to the results obtained in our experimental study and our computational single-cell model. Their finding that the effect of A293 on AERPs was even more pronounced in the Alessi goat model of tachypacing-induced artificial AF is most likely explained by AF-associated upregulation of TASK-1, as K_v1.5 was described to be downregulated in atrial remodeling.³⁶

CLINICAL IMPLICATIONS

In addition to the atrial myocardium, TASK-1 is expressed in human pulmonary artery smooth muscle cells.³⁷ In these cells, TASK-1 currents are crucial for setting the basal membrane potential and consecutively regulating pulmonary vascular tone.³⁸ Additionally, TASK-1 loss-of-function mutations were identified in patients suffering from idiopathic pulmonary arterial hypertension.³⁹ Experimental results on the effects of TASK-1 inhibition on the pulmonary arterial vascular tone, however, are extremely sparse and partially contradicting. While rats were reported to exhibit pulmonary arterial hypertension after chronic exposure to a TASK-1 inhibitor,⁴⁰ TASK-1 knockout mice displayed pulmonary artery pressure and right ventricular pressure levels that did not differ from their wild-type littermates.^{41,42} Further studies will be necessary to clarify whether pharmacologic TASK-1 inhibition leads to pulmonary arterial hypertension and to explore its long-term efficacy, safety, and toxicology. In our study, A293 treatment was well tolerated in sedated animals. After drug exposure, no clinical adverse effects were observed over a period of 3 to 5 days.

LIMITATIONS

It is, however, very important to consider that the AF subtype simulated in our porcine arrhythmia model is a relatively mild form of AF that might lack significant structural alterations of atrial tissue that contribute to the development and maintenance of arrhythmia in AF patients. While our results might be cautiously extrapolated



to situations with new onset of paroxysmal AF episodes, they cannot be generalized to patients suffering from persistent AF. In the past, for instance, blockers of the $K_v1.5$ channel were found to display robust antiarrhythmic effects during sinus rhythm, which were significantly attenuated under AF conditions attributable to functional ion channel remodeling and structural alterations.¹⁷

Therefore, further studies will need to assess the performance of TASK-1 inhibition in acute

cardioversion of persistent AF. Further, the efficacy of TASK-1 current inhibition in rhythm control of persistent AF remains to be elucidated. Finally, as AF-related upregulation of TASK-1 currents was reported in human^{10,11} as well as in porcine disease models,^{43,44} one could speculate that TASK-1 inhibition exerts antiarrhythmic potential, especially in patients with persistent AF. The fact that human atrial cardiomyocytes display slightly higher TASK-1 current densities than

Figure 6. Computational modeling of the effect of A293 on atrial electrophysiology in single-cell and tissue model.

A through **C**, Single-cell model simulations of actions potentials and APD for different BCL values and A293 concentrations. **A**, Simulated APs are depicted at 4 BCLs in absence of A293 (solid line) or complete inhibition of TASK-1 channels by A293 (dashed line) (**B**) APD at 90% repolarization (APD₉₀) dependent on the concentration of A293 (IC₅₀ of 100 nmol/L) at the four different BCLs. Boxplots depicting APD₉₀ values obtained from patch clamp experiments under control conditions (CTRL) and after application of 200 nmol/L A293 are provided as inserts. **C**, Predicted relative change of APD₉₀ dependent on the concentration of A293. **D** through **F**, Arrhythmia termination by A293 in a simplified model of the left atrium. **D**, *Black spheres*: geometrical model consisting of a spherical surface (diameter of 5 cm) with 5 orifices representing the left and right inferior and superior pulmonary veins (LIPV/RIPV/LSPV/RSPV) as well as the mitral valve annulus. The blue box in (**D**) indicates the last 150 ms of the 10 s control period simulation advancing the final 5 seconds depicted in (**E**) and (**F**). **E**, Representative snapshots of the final 5 s simulation without TASK-1 inhibition by A293. The rotor continues to exist in the left atrial model. **F**, Same snapshots as in (**E**) but including the effect of A293 in the model. The meandering of the rotor increases and APD alternans starts. Following a rotor with long APD, the final rotor interacts with the waveback of the one before and a termination of the arrhythmia is occurring. Simulations were performed for a tissue conductivity of 1.0 S/m. Colors from black (−80 mV) to red (10 mV) indicate the transmembrane voltage (TMV) as depicted in the scalebar. APD indicates action potential duration; BCL, basic cycle length; and TASK-1, TWIK-related acid-sensitive K⁺ channel.

those of pigs may indicate a pronounced antiarrhythmic efficacy of TASK-1 current inhibition in patients. Furthermore, remodeling of TASK-1 channels differs between AF subgroups with preserved or reduced left ventricular ejection fraction,¹¹ providing a mechanistic basis for an individualized pharmacotherapy of AF.

The sample sizes used in this study were relatively small because of regulations on animal protection. It was reported that members of the K_{2P} family are susceptible to a wide range of narcotics. Therefore, propofol was used as an anesthetic agent in this study because its effect on TASK-1 had been ruled out in previous studies.⁴⁴

CONCLUSIONS

In conclusion, pharmacologic TASK-1 inhibition by A293 prolongs atrial refractoriness with no effects on ECG intervals and ventricular repolarization. Therefore, blockade of atrial TASK-1 currents exerts class III antiarrhythmic effects in vivo, resulting in acute cardioversion of paroxysmal AF episodes. Finally, our results confirmed the role of TASK-1 as a promising drug target in AF and might therefore promote the translation of a novel, mechanism-based antiarrhythmic paradigm into clinical practice.

ARTICLE INFORMATION

Received December 23, 2019; accepted April 3, 2020.

Affiliations

From the Department of Cardiology (F.W., C.B., A.B., M.Kr., J.N., D.T., H.A.K., C.S.), DZHK (German Center for Cardiovascular Research), partner site Heidelberg/Mannheim (F.W., X.Z., M.Kr., D.T., M.B., H.A.K., C.S.), and HCR Heidelberg Center for Heart Rhythm Disorders (F.W., C.B., A.B., M.Kr., J.N., D.T., H.A.K., C.S.), University of Heidelberg, Germany; First Department of Medicine, University Medical Center Mannheim, Germany (X.Z., M.B.); Institute for Experimental Cardiovascular Medicine, University Heart Center Freiburg, Bad Krozingen, Germany (T.P.W., G.S.); Medical Center University of Freiburg, and Faculty of Medicine, University of Freiburg, Germany (T.P.W., G.S.); Institute of Biomedical Engineering, Karlsruhe Institute of Technology (KIT), Karlsruhe, Germany (L.A.U., A.L.);

Department of Cardiac Surgery, University Hospital Heidelberg, Germany (B.S., M.Ka.); Department of Cardiac Surgery, University Hospital Essen, Germany (A.R.).

Acknowledgments

We thank Sabine Höllriegel, Patricia Kraft, Katrin Kupser and Kai Sonja for excellent technical support.

Sources of Funding

This work was supported by research grants from the University of Heidelberg, Faculty of Medicine (Rahel Goitein-Straus Scholarship and Olympia-Morata Scholarship to Schmidt); from the German Center for Cardiovascular Research (DZHK) (Excellence Grant to Schmidt, Postdoc Startup Grant to Wiedmann); from the German Cardiac Society (DGK) (Research Scholarship DGK082018 to Wiedmann, Otto-Hess Fellowship to Wiedmann); from the German Heart Foundation/German Foundation of Heart Research (F/15/18 to Wiedmann, F/41/15 to Schmidt, Kaltenbach Scholarship to Büscher and Wiedmann); from the Ministry of Science, Research and the Arts Baden-Wuerttemberg (Sonderlinie Medizin to Thomas); from the Joachim-Herz Foundation (Addon-Fellowship for interdisciplinary life sciences to Wiedmann) and from the German Research Foundation (DFG) (LO 2093/1-1 to Loewe, SCHM 3358/1-1 to Schmidt, SE 1758/3-3 to Seemann TH 1120/7-1 to Thomas).

Disclosures

None.

Supplementary Materials

Video S1

Video S2

Video S3

REFERENCES

- Kirchhof P, Benussi S, Kotecha D, Ahlsson A, Atar D, Casadei B, Castella M, Diener HC, Heidbuchel H, Hendriks J, et al. 2016 ESC Guidelines for the management of atrial fibrillation developed in collaboration with EACTS. *Europace*. 2016;18:1609–1678.
- Fabritz L, Guasch E, Antoniades C, Bardinet I, Benninger G, Betts TR, Brand E, Breithardt G, Bucklar-Suchankova G, Camm AJ, et al. Expert consensus document: defining the major health modifiers causing atrial fibrillation: a roadmap to underpin personalized prevention and treatment. *Nat Rev Cardiol*. 2016;13:230–237.
- January CT, Wann LS, Calkins H, Chen LY, Cigarroa JE, Cleveland JC Jr, Ellnor PT, Ezekowitz MD, Field ME, Furie KL, et al. 2019 AHA/ACC/HRS focused update of the 2014 AHA/ACC/HRS guideline for the management of patients with atrial fibrillation: a report of the American College of Cardiology/American Heart Association Task Force on Clinical Practice Guidelines and the Heart Rhythm Society. *J Am Coll Cardiol*. 2019;47:104–132.
- Goldstein SAN, Bockenhauer D, O'Kelly I, Zilberberg N. Potassium leak channels and the KCNK family two-P-domain subunits. *Nat Rev Neurosci*. 2001;2:175–184.

5. Patel AJ, Honoré E. Molecular physiology of oxygen-sensitive potassium channels. *Eur Respir J*. 2001;18:221–227.
6. Bayliss DA, Barrett PQ. Emerging roles for two-pore-domain potassium channels and their potential therapeutic impact. *Trends Pharmacol Sci*. 2008;29:566–575.
7. Lloyd EE, Crossland RF, Phillips SC, Marrelli SP, Reddy AK, Taffet GE, Hartley CJ, Bryan RM Jr. Disruption of $K_{2p}6.1$ produces vascular dysfunction and hypertension in mice. *Hypertension*. 2011;58:672–678.
8. Schmidt C, Wiedmann F, Schweizer PA, Becker R, Katus HA, Thomas D. Class I antiarrhythmic drugs inhibit human cardiac two-pore-domain K^+ (K_{2p}) channels. *Eur J Pharmacol*. 2013;721:237–248.
9. Kim D, Kang D. Role of K_{2p} channels in stimulus-secretion coupling. *Pflugers Arch*. 2015;467:1001–1011.
10. Schmidt C, Wiedmann F, Voigt N, Zhou XB, Heijman J, Lang S, Albert V, Kallenberger S, Ruhparwar A, Szabó G, et al. Upregulation of $K_{2p}3.1$ K^+ current causes action potential shortening in patients with chronic atrial fibrillation. *Circulation*. 2015;132:82–92.
11. Schmidt C, Wiedmann F, Zhou XB, Heijman J, Voigt N, Ratte A, Lang S, Kallenberger SM, Campana C, Weymann A, et al. Inverse remodeling of $K_{2p}3.1$ K^+ channel expression and action potential duration in left ventricular dysfunction and atrial fibrillation: implications for patient-specific antiarrhythmic drug therapy. *Eur Heart J*. 2017;38:1764–1774.
12. Limberg SH, Netter MF, Rolfes C, Rinné S, Schlichthörl G, Zuzarte M, Vassiliou T, Moosdorf R, Wulf H, Daut J, et al. TASK-1 channels may modulate action potential duration of human atrial cardiomyocytes. *Cell Physiol Biochem*. 2011;28:613–624.
13. Rinné S, Kiper AK, Schlichthörl G, Dittmann S, Netter MF, Limberg SH, Silbernagel N, Zuzarte M, Moosdorf R, Wulf H, et al. TASK-1 and TASK-3 may form heterodimers in human atrial cardiomyocytes. *J Mol Cell Cardiol*. 2015;81:71–80.
14. Schmidt C, Wiedmann F, Langer C, Tristram F, Anand P, Wenzel W, Lugenbiel P, Schweizer P, Katus HA, Thomas D. Cloning, functional characterization, and remodeling of $K_{2p}3.1$ (TASK-1) potassium channels in a porcine model of atrial fibrillation and heart failure. *Heart Rhythm*. 2014;11:1798–1805.
15. Schmidt C, Wiedmann F, Tristram F, Anand P, Wenzel W, Lugenbiel P, Schweizer P, Katus HA, Thomas D. Therapeutic targeting of two-pore-domain potassium (K_{2p}) channels in the cardiovascular system. *Clin Sci (Lond)*. 2016;130:643–650.
16. Putzke C, Wemhöner K, Sachse FB, Rinné S, Schlichthörl G, Li XT, Jaé L, Eckhardt I, Wischmeyer E, Wulf H, et al. The acid-sensitive potassium channel TASK-1 in rat cardiac muscle. *Cardiovasc Res*. 2007;75:59–68.
17. Kiper AK, Rinné S, Rolfes C, Ramírez D, Seeböhm G, Netter MF, González W, Decher N. $Kv1.5$ blockers preferentially inhibit TASK-1 channels: TASK-1 as a target against atrial fibrillation and obstructive sleep apnea? *Pflugers Arch*. 2015;467:1081–1090.
18. Wiedmann F, Kiper AK, Bedoya M, Ratte A, Rinné S, Kraft M, Waibel M, Anand P, Wenzel W, Gonzalez W, et al. Identification of the A293 (AVE1231) binding site in the cardiac two-pore-domain potassium channel TASK-1: a common low affinity antiarrhythmic drug binding site. *Cell Physiol Biochem*. 2019;52:1223–1235.
19. Bazett HC. An analysis of time relations of electrocardiograms. *Heart*. 1920;7:353–367.
20. Wiedmann F, Schlund D, Voigt N, Ratte A, Kraft M, Katus HA, Schmidt C. N-glycosylation-dependent regulation of $hK_{2p}17.1$ currents. *Mol Biol Cell*. 2019;30:1425–1436.
21. Wiedmann F, Schulte JS, Gomes B, Zafeiriou M-P, Ratte A, Rathjens F, Fehrmann E, Scholz B, Voigt N, Müller FU, et al. Atrial fibrillation and heart failure-associated remodeling of two-pore-domain potassium (K_{2p}) channels in murine disease models: focus on TASK-1. *Basic Res Cardiol*. 2018;113:27.
22. Lolicato M, Arrigoni C, Mori T, Sekioka Y, Bryant C, Clark KA, Minor DL Jr. $K_{2p}2.1$ (TREK-1)-activator complexes reveal a cryptic selectivity filter binding site. *Nature*. 2017;547:364–368.
23. Biasini M, Bienert S, Waterhouse A, Arnold K, Studer G, Schmidt T, Kiefer F, Cassarino TG, Bertoni M, Bordoli L, et al. SWISS-MODEL: modelling protein tertiary and quaternary structure using evolutionary information. *Nucleic Acids Res*. 2014;42:W252–W258.
24. Kiefer F, Arnold K, Künzli M, Bordoli L, Schwede T. The SWISS-MODEL repository and associated resources. *Nucleic Acids Res*. 2009;37:D387–D392.
25. Arnold K, Bordoli L, Kopp J, Schwede T. The SWISS-MODEL Workspace: a web-based environment for protein structure homology modelling. *Bioinformatics*. 2006;22:195–201.
26. Guex N, Peitsch MC, Schwede T. Automated comparative protein structure modeling with SWISS-MODEL and Swiss-PdbViewer: a historical perspective. *Electrophoresis*. 2009;30:S162–S173.
27. Trott O, Olson AJ. AutoDock Vina: improving the speed and accuracy of docking with a new scoring function, efficient optimization, and multithreading. *J Comput Chem*. 2010;31:455–461.
28. Morris GM, Huey R, Lindstrom W, Sanner MF, Belew RK, Goodsell DS, Olson AJ. AutoDock4 and AutoDockTools4: automated docking with selective receptor flexibility. *J Comput Chem*. 2009;30:2785–2791.
29. Courtemanche M, Ramirez RJ, Nattel S. Ionic mechanisms underlying human atrial action potential properties: insights from a mathematical model. *Am J Physiol*. 1998;275:H301–H321.
30. Wilhelms M, Hettmann H, Maleckar MM, Koivumäki JT, Dössel O, Seemann G. Benchmarking electrophysiological models of human atrial myocytes. *Front Physiol*. 2013;3:487.
31. Vigmond EJ, Weber dos Santos R, Prassl AJ, Deo M, Plank G. Solvers for the cardiac bidomain equations. *Prog Biophys Mol Biol*. 2007;96:3–18.
32. Unger L, Oesterlein T, Seemann G, Dössel O, Spector P, Loewe A. Estimating refractory periods during atrial fibrillation based on electrogram cycle lengths in a heterogeneous simulation setup. *Curr Dir Biomed Eng*. 2017;3:317–320.
33. Matene E, Jacquemet V. Fully automated initiation of simulated episodes of atrial arrhythmias. *Europace*. 2012;14(suppl 5):v17–v24.
34. Ravens U. Novel pharmacological approaches for antiarrhythmic therapy. *Naunyn Schmiedeberg Arch Pharmacol*. 2007;381:187–193.
35. Wirth KJ, Brendel J, Steinmeyer K, Linz DK, Rütten H, Gögelein H. In vitro and in vivo effects of the atrial selective antiarrhythmic compound AVE1231. *J Cardiovasc Pharmacol*. 2007;49:197–206.
36. Voigt N, Dobrev D. Ion channel remodeling in atrial fibrillation. *Eur Cardiol*. 2011;7:97–103.
37. Olschewski A, Chandran N, Olschewski H. Letter by Olschewski et al. Regarding Article, “Upregulation of $K_{2p}3.1$ K^+ Current Causes Action Potential Shortening in Patients With Chronic Atrial Fibrillation”. *Circulation*. 2016;133:e439.
38. Olschewski A, Li Y, Tang B, Hanze J, Eul B, Bohle RM, Wilhelm J, Morty RE, Brau ME, Weir EK, et al. Impact of TASK-1 in human pulmonary artery smooth muscle cells. *Circ Res*. 2006;98:1072–1080.
39. Ma L, Roman-Campos D, Austin ED, Eyries M, Sampson KS, Soubrier F, Germain M, Tréguet DA, Borczuk A, Rosenzweig EB, et al. A novel channelopathy in pulmonary arterial hypertension. *N Engl J Med*. 2013;69:351–361.
40. Antigny F, Hautefort A, Meloche J, Belacel-Ouari M, Manoury B, Rucker-Martin C, Péchoux C, Potus F, Nadeau V, Tremblay E, et al. Potassium channel subfamily K member 3 (KCNK3) contributes to the development of pulmonary arterial hypertension. *Circulation*. 2016;133:1371–1385.
41. Murtaza G, Mermer P, Goldenberg A, Pfeil U, Paddenberg R, Weissmann N, Lochnit G, Kummer W. TASK-1 potassium channel is not critically involved in mediating hypoxic pulmonary vasoconstriction of murine intra-pulmonary arteries. *PLoS One*. 2017;12:e0174071.
42. Kitagawa MG, Reynolds JO, Wehrens XHT, Bryan RM, Pandit LM. Hemodynamic and pathologic characterization of the TASK-1^{-/-} mouse does not demonstrate pulmonary hypertension. *Front Med (Lausanne)*. 2017;4:177.
43. Schmidt C, Wiedmann F, Beyersdorf C, Zhao Z, El-Battrawy I, Lan H, Szabo G, Li X, Lang S, Korkmaz-Icoz S, et al. Genetic ablation of TASK-1 (Tandem of P Domains in a Weak Inward Rectifying K^+ Channel-Related Acid-Sensitive K^+ Channel-1) ($K_{2p}3.1$) K^+ channels suppresses atrial fibrillation and prevents electrical remodeling. *Circ Arrhythm Electrophysiol*. 2019;12:e007465.
44. Putzke C, Hanley PJ, Schlichthörl G, Preisig-Müller R, Rinné S, Anetseder M, Eckenhoff R, Berkowitz C, Vassiliou T, Wulf H, et al. Differential effects of volatile and intravenous anesthetics on the activity of human TASK-1. *Am J Physiol Cell Physiol*. 2007;293:C1319–C1326.